JOURNAL OF COMPUTATIONAL PHYSICS 48, 72–105 (1982)

Solution of Burner-Stabilized Premixed Laminar Flames by Boundary Value Methods

MITCHELL D. SMOOKE

Sandia National Laboratories, Livermore, CA 94550

Received February 17, 1982

A numerical technique has been developed for integrating the one-dimensional steady state premixed laminar flame equations. A global finite difference approach is used in which the nonlinear difference equations are solved by a damped-modified Newton method. An assumed temperature profile helps to generate a converged numerical solution on an initial coarse grid. Mesh points are inserted in regions where the solution profiles exhibit high gradient and high curvature activity. These features are discussed and illustrated in the paper, and the method is used to calculate the temperature and species profiles of several laboratory flames.

1. INTRODUCTION

Laminar premixed flames (flat flames) are commonly used to investigate chemical kinetics processes that are important in combustion. Because of its essentially one-dimensional nature, the flat flame is particularly useful in constructing computational models. In close conjunction with experimental data, these models can provide detailed information on flame structure and elementary reaction paths. The underlying reason for working with these models is that they will ultimately enable one to propose measures that can reduce pollutant formation and thus provide cleaner combustion. For example, flat flame studies can aid in understanding the production of nitric oxide (NO) in ammonia-oxygen (NH_3–O_2) flames and in the prediction of the onset of soot formation in acetylene-oxygen (C_2H_2–O_2) flames [1].

Premixed laminar flames are obtained in the laboratory (see Fig. 1) by flowing premixed fuel and oxidizer through a cooled porous plate. Since in general there is a positive temperature gradient at the origin due to heat transfer from the burning mixture back to the burner, the flame is nonadiabatic. (In the adiabatic case, the flame sits infinitely far from the burner with a zero temperature gradient at the burner.) Because the flat flame is an excellent configuration on which to apply diagnostic techniques, these flames are common in combustion laboratories and, as a result, a great deal of experimental data is available. In addition, one can adjust the fuel-to-oxidizer ratio to form fuel-rich or fuel-lean flames and adjust the pressure to narrow or widen the flame zone.

The calculation of laminar premixed flames was one of the first combustion problems to be attacked by both analytical and numerical techniques. Although the

0021-9991/82/100072-34$02.00/0

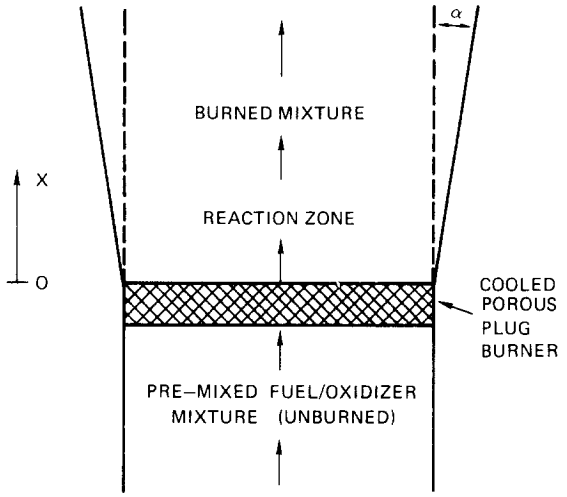

FIG. 1. Schematic of nonadiabatic premixed laminar flame. The flame gases expand as a function of the height x above the burner; the angle α is the expansion angle.

problem has a very simple flow configuration, the numerical solution of the governing equations has proved to be difficult and is still being actively pursued. In this paper, we develop a numerical method which enables us to integrate the steady state, laminar, one-dimensional, premixed flame equations. A global finite difference approach is used in which the nonlinear difference equations are solved by a damped-modified Newton method. The combination of an assumed temperature profile and upwind differencing of the convective terms helps to generate a converged numerical solution to the species equations on an initial coarse grid. This solution is then used as an initial starting estimate for the species, or energy and species, equations on a finer mesh. Grid points are inserted in regions where the solution profiles exhibit high gradient and high curvature activity.

In the next section, we review the approaches that have been used to obtain numerical solutions of the premixed flame equations. In Section 3, we introduce some notation and formulate the premixed flame problem as a nonlinear two-point boundary value problem. In Section 4 we present the boundary value method we have used to solve the flame equations and Section 5 contains the results of applying our method to several laboratory flames.

2. BACKGROUND

One of the first attempts to solve the premixed flame equations was by Hirschfelder and his co-workers [2]. They applied a combination of linear asymptotic analysis and a numerical shooting method to obtain temperature and species profiles

together with the adiabatic flame speed for several simple flames. In 1956, Spalding [3] solved the equations governing the adiabatic problem by considering the problem as a relaxation of a time-dependent system of nonlinear parabolic partial differential equations. Assuming initial profiles for the temperature and species concentrations, Spalding discretized the equations using standard finite difference techniques; the solution was advanced in time by a marching procedure until steady state profiles were obtained. Time-dependent procedures have since been used in adiabatic problems, for example, by Adams and Cook [4] in studying the effect of pressure on the mechanism and speed of hydrazine flames, by Dixon–Lewis [5] in studying hydrogen-oxygen flames and by Westbrook and Dryer [6, 7] in predicting laminar flame properties of methanol-air mixtures. A time-dependent method for the general nonadiabatic case was introduced in 1971 by Spalding and Stephenson [8]. In a somewhat related approach, Bledjian [9] employed a method of lines technique to solve the adiabatic problem. In this method, the spatial coordinate is discretized and the original nonlinear parabolic mixed initial-boundary value problem is reduced to a set of nonlinear first-order initial value problems. Sophisticated initial value problem integrators can then be used to integrate the resulting ordinary differential equation system. More recently, Margolis [10] has used a method of lines technique employing spline collocation in the spatial variable to solve the equations governing the adiabatic and nonadiabatic cases.

Although the literature contains numerous examples of the use of time-dependent methods to investigate flat flame structure, there are relatively few references to the solution of the flame equations by steady state or time-independent methods. Dixon–Lewis [11] has applied a combination of time-dependent and time-independent methods in calculating the structure of certain flames and Wilde [12] and Kendall and Kelly [13] have been successful in applying a strictly time-independent method to solve the premixed flame equations. Wilde solved the governing equations by employing a combination of quasilinearization and orthonormalization, where the fundamental solution matrix was constructed analytically over appropriate intervals. Both Wilde and Kendall and Kelly have also applied finite difference methods to solve the governing equations. Our work is an extension of the approaches used by Wilde, and Kendall and Kelly.

Although time-dependent methods have been used with greater frequency and with greater success in solving premixed laminar flames than have steady state methods, the slow relaxation of the time-dependent solution to steady state can make parameter studies employing complicated nonlinear transport properties extremely time consuming. By dealing directly with the governing equations, however, steady state methods have the potential to solve the flame equations in a fraction of the time taken by time-dependent methods.

Difficulties with Using Steady State Methods

Of the various methods for solving two-point boundary value problems, those that have been implemented in most of the currently available two-point boundary value

problem software can be classified as either initial value (shooting type) methods [14–16] or global methods such as finite differences [17] and collocation [18].

The availability of initial value problem software and the relative ease of implementing shooting type methods have made them particularly appealing for numerically solving two-point boundary value problems. In addition, with variable step initial value problem integrators, one can accurately resolve rapidly changing components of the dependent solution variables. For these reasons, many of the early attempts to solve the premixed flame equations by steady state methods [2, 11, 12] incorporated some form of initial value technique.

Shooting methods are based upon the equivalence existing between the given boundary value problem and a related initial value problem. To use shooting methods effectively, it is essential that small changes in the initial conditions of the initial value problem should result in small changes in the initial value solution. Such problems are considered to be stable or well posed. Problems which do not exhibit such behavior are said to be ill-conditioned or unstable. This type of instability is inherent in the problem and does not depend upon the initial value problem integrator, although it is possible that the numerical integrator itself may be a source of instability. Techniques such as multiple shooting [19], continuation [20], and orthonormalization [16] have all been used to reduce the sensitivity of such problems to small changes in the initial conditions.

When shooting methods (such as the method of adjoints or the method of complementary functions [20]) are implemented in practice, a set of linear equations must be solved for a set of missing initial conditions (linear problems) or for corrections to a set of missing initial conditions (nonlinear problems). For the linear equations to have a unique solution, it is necessary that the columns of the coefficient matrix of the system be numerically linearly independent. Although the columns of the matrix of coefficients formed by the method of adjoints or the method of complementary functions are linearly independent initially, in numerically sensitive problems, they may rapidly become numerically linearly dependent as the integration proceeds. This is particularly true when the eigenvalues of the $n \times n$ matrix $A(t)$ in linear problems of the form $y' = A(t)y + g(t)$, or the $n \times n$ Jacobian matrix $J(y) = \partial f/\partial y$ in nonlinear problems of the form $y' = f(t, y)$, have eigenvalues well separated in numerical value. In both problems y, y', g, and f are n-vectors.

In a recent paper, Margolis [21] shows that for a simple flame involving three species, temperature, and a global two step reaction mechanism, an asymptotic analysis reveals solutions of the premixed flame equations which both grow and decay exponentially. The exponential solutions result from the presence of locally positive and locally negative eigenvalues in the coefficient matrix of the linearized flame equations. Margolis shows that some of these eigenvalues are proportional to the square root of expressions similar to the rate constants in Eq. (3.15). Although the solutions corresponding to locally positive eigenvalues are unphysical, they can be excited by round-off error when the premixed flame problem is solved by an initial value method. Even though the analysis carried out in [21] was applied to a simple model flame, it is reasonable to expect that a similar analysis applied to laboratory

flames with complex chemical kinetics mechanisms will produce analogous results. In particular, for a fuel-rich, low pressure hydrogen-oxygen (H_2–O_2) flame [22], we have found the eigenvalues of the coefficient matrix of the variational equations to be as large as 500. A simple analysis shows that if such a flame were solved by a multiple shooting method on a 16 digit machine, we could expect on the order of one hundred shooting points. Our numerical experience has indeed confirmed such a result.

From the above discussion, it is clear that the solution of premixed flame problems by initial value methods is not the way to proceed. If premixed flame structure is to be calculated using steady state methods, the methods must be global. Finite differences and collocation are two logical choices. These methods incorporate both the specified initial and terminal conditions into the set of linear or nonlinear equations that must be solved to obtain approximations to the soluion of the original differential equations. Experience has shown that they can be used with considerable success in solving numerically sensitive two-point boundary value problems [20, 23, 24].

Two currently available global two-point boundary value problem codes are PASVA3 [17] and COLSYS [18]. The PASVA3 code, written by Lentini and Pereyra, is a finite difference code employing deferred corrections. The COLSYS code, as implemented by Ascher, Christiansen, and Russell, is a collocation package designed for solving mixed order systems of multipoint boundary value problems. In addition to being able to handle numerically sensitive problems, both these codes adaptively adjust the grid spacing so as to be able to resolve high gradient activity of the dependent solution components.

In the course of our work, we applied both PASVA3 and COLSYS to a very simple three species and temperature flame. The difficulty in obtaining a converged numerical solution for our prescribed initial solution estimates combined with the large amount of storage overhead needed to solve the test problem made it clear that the usefulness of these codes in determining the structure of laboratory flames would be minimal. We believe, however, that in many other applications the use of general purpose codes such as PASVA3 and COLSYS is often preferable to writing one's own code.

From the above discussion, it is clear why steady state methods have not been applied with much success in solving premixed laminar flames. In spite of these difficulties, we feel that the potential advantages to be gained in using such methods make their investigation well worthwhile. The method that we develop in this paper helps to eliminate many of the difficulties that have been associated with using steady state methods to solve the premixed flame equations.

3. Problem Formulation

Our formulation of the burner-stabilized flame problem closely follows that originally proposed by Hirschfelder and Curtiss [25]. The physical problem is

illustrated in Fig. 1. A premixed fuel and oxidizer mixture flows through a cooled porous plug burner. As the mixture emerges from the burner, it passes through a reaction zone in which chemical changes take place. Further downstream, it eventually emerges in a burned state. Our goal is to be able to predict theoretically the mass fractions Y_k, $k = 1, 2,..., N$, of the species under investigation, and T, the temperature of the combustible mixture, as functions of the height x above the burner. Our formulation of the problem assumes the following: (i) The flow is one-dimensional and the region under consideration is the semi-infinite interval $0 \leqslant x < \infty$. (ii) For normal laboratory flames, the flow velocities are small and hence viscous effects are negligible. This assumption allows the momentum equation to be integrated and replaced by the condition that the thermodynamic pressure p is constant. (iii) We allow for the possible quasi-one-dimensional expansion of the flame gases, where $A(x)$ represents the cross-sectional area of the flame as a function of the height x above the burner. (iv) Body forces are negligible. (v) Radiative heat transfer is negligible. (vi) The diffusion of heat due to concentration gradients (Dufour effect) is negligible.

With approximations (i)–(vi), the equations governing the structure of a steady one-dimensional isobaric flame are:

(a) continuity,

$$\dot{M} = \rho u A = \text{const.}, \tag{3.1}$$

(b) conservation of species,

$$\dot{M}(dY_k/dx) = -(d/dx)(\rho A Y_k V_k) + \dot{w}_k A W_k, \qquad k = 1, 2,..., N, \tag{3.2}$$

(c) conservation of energy,

$$\dot{M}\frac{dT}{dx} = \frac{1}{C_p}\frac{d}{dx}\left(\lambda A \frac{dT}{dx}\right) - \frac{A}{C_p}\left[\sum_{k=1}^{N} \rho Y_k V_k C_{pk}\right]\frac{dT}{dx} - \frac{A}{C_p}\sum_{k=1}^{N} \dot{w}_k h_k W_k, \tag{3.3}$$

(d) equation of state,

$$\rho = \bar{W}p/RT, \tag{3.4}$$

with the boundary conditions:

$$T(0) = T_b, \tag{3.5}$$

$$Y_k + (\rho Y_k V_k A/\dot{M}) = \varepsilon_k, \qquad k = 1, 2,..., N, \tag{3.6}$$

$$dT/dx = 0, \qquad \text{as} \quad x \to \infty, \tag{3.7}$$

$$dY_k/dx = 0, \qquad \text{as} \quad x \to \infty, \quad k = 1, 2,..., N. \tag{3.8}$$

In addition to the variables already defined, u denotes the velocity of the fluid mixture, ρ the density of the fluid mixture, W_k the molecular weight of the kth

species, $\bar{W}$ the mean molecular weight of the mixture, R the universal gas constant, λ the thermal conductivity of the mixture, C_p the specific heat capacity of the mixture at constant pressure, C_{pk} the specific heat capacity at constant pressure of the kth species, $\dot{w}_k$ the rate of production of the kth species by chemical reaction, h_k the specific enthalpy of the kth species with respect to the mixture of remaining species, ε_k the known incoming mass flux fractions, and V_k the binary diffusion velocity of the kth species.

The diffusion velocity is divided into three parts

$$V_k = v_k + w_k + v_c, \qquad k = 1, 2,..., N, \tag{3.9}$$

where v_k is the ordinary diffusion velocity due to mole fraction gradients, w_k is the thermal diffusion velocity, and v_c is a constant diffusion velocity (independent of species). We approximate v_k by the Curtiss–Hirschfelder [26] approximation. We write

$$v_k = -(1/X_k)\, D_k \nabla X_k, \qquad k = 1, 2,..., N, \tag{3.10}$$

where X_k is the mole fraction of the kth species and D_k is related to the binary diffusion coefficients $\mathscr{D}_{jk}$ through the relation

$$D_k = (1 - Y_k) \Big/ \left(\sum_{j \neq k} X_j / \mathscr{D}_{jk} \right). \tag{3.11}$$

Thermal diffusion is incroporated into the model only in the trace light component limit. The thermal diffusion velocity is given by

$$w_k = (D_k t_{D_k} / X_k)(1/T)\, dT/dx, \tag{3.12}$$

where t_{D_k} is the thermal diffusion coefficient of species k. We only apply Eq. (3.12) for low molecular weight species such as H, H_2, or He. The constant diffusion velocity v_c is introduced in order to satisfy the condition

$$\sum_{k=1}^{N} V_k Y_k = 0, \tag{3.13}$$

which must be satisfied if mass is guaranteed to be conserved. Upon making use of Eqs. (3.9) and (3.13) we have

$$v_c = -\sum_{k=1}^{N} Y_k (w_k + v_k). \tag{3.14}$$

The transport model we use is essentially the same as that recommended by Coffee and Heimerl [27]. The multicomponent conductivity is computed from the single component conductivities using Wilke's semiempirical formula [28], and an approximate Eucken–Hirschfelder correction for polyatomic species is incorporated in the

single component conductivities in the manner followed by Svehla [29]. The thermal diffusion coefficients are calculated using the thermal diffusion ratio discussed in Chapman and Cowling [30].

The production rate $\dot{w}_k$ for the kth species can be written in the form

$$\dot{w}_k = \sum_{j=1}^{m} (v_{jk}^P - v_{jk}^R) \left[k_j^f(T) \prod_{n=1}^{N} \left(\frac{\rho Y_n}{W_n} \right)^{v_{jn}^R} - k_j^r(T) \prod_{n=1}^{N} \left(\frac{\rho Y_n}{W_n} \right)^{v_{jn}^P} \right], \tag{3.15}$$

where $v_{jk}^R(v_{jk}^P)$ is the stoichiometric coefficient of species k appearing as a reactant (product) in reversible reaction j, $j = 1, 2,..., m$. The function $k_j^f(k_j^r)$ is the rate constant for the forward (reverse) path of reaction j. We assume k_j^f has the following modified Arrhenius temperature dependence:

$$k_j^f = A_j^f T^{\beta_j^f} e^{-(E_j^f/RT)}, \tag{3.16}$$

and similarly for k_j^r. The reverse rate constants k_j^r can be written in terms of the forward rate constants and the equilibrium constants k_j^c by

$$k_j^r = k_j^f / k_j^c. \tag{3.17}$$

The pre-exponential factor A_j^f, the exponent β_j^f, the activation energy E_j^f, and similar expressions for the reverse reaction quantities can be compiled from published experimental work.

4. Method of Solution

We recall that the premixed flame problem is formulated as a nonlinear two-point boundary value problem on the semi-infinite interval $0 \leqslant x < \infty$. If the problem were linearized about the burned state values of the temperature and the species mass fractions (T^b and Y_k^b, $k = 1, 2,..., N$), then we would say that the point $x = \infty$ is a singularity of the second kind having rank one. The most common approach to handle the point $x = \infty$ is to solve the governing equations on the finite interval $0 \leqslant x \leqslant L$ for some number $L < \infty$ with the boundary conditions at ∞ imposed at $x = L$.

In recent years, several papers have been written which discuss the choice of the proper asymptotic boundary conditions when a two-point boundary value problem posed on an infinite interval is solved on a finite interval [31–33]. In all of these projection type methods, an a priori knowledge of the asymptotic value of the dependent solution vector is required. In adiabatic flames, we can obtain the burned state for both the temperature and the species under investigation. This information, however, is generally not known for burner-stabilized flames. As such, we have chosen to apply the zero flux boundary conditions at $x = L$. The appropriate value of L can be obtained from experiment or from a small amount of numerical computation.

Newton's Method

Our goal is to obtain a discrete solution of Eqs. (3.1)–(3.8) on the mesh $\mathcal{M}$,

$$\mathcal{M} = \{0 = x_0 < x_1 < \cdots < x_M = L\}, \tag{4.1}$$

where $h_j = x_j - x_{j-1}$, $j = 1, 2,..., M$, and $h = \max_{1 \leqslant j \leqslant M} h_j$.

We approximate the spatial derivatives in Eqs. (3.1)–(3.8) using finite difference expressions. In particular, the diffusion terms in Eqs. (3.2) and (3.3) are approximated using central differences—that is, we write

$$\frac{\partial}{\partial x}\left(a(x)\frac{\partial g}{\partial x}\right)\bigg|_{x_j} \cong \left(\frac{2}{x_{j+1} - x_{j-1}}\right)(a^{j+1/2}\,\partial g^{j+1} - a^{j-1/2}\,\partial g^j), \tag{4.2}$$

where for a continuous mapping $g: [0, L] \to \mathrm{R}^1$, we define $g^j = g(x_j)$, $j = 0, 1,..., M$, and

$$g^{j+1/2} = (g^{j+1} + g^j)/2, \qquad j = 0, 1,..., M-1, \tag{4.3}$$

$$\partial g^{j+1} = (g^{j+1} - g^j)/h_{j+1}, \qquad j = 0, 1,..., M-1. \tag{4.4}$$

The convective derivatives and the remaining terms which contain first derivatives are all differenced using upwind difference expressions. We write

$$\frac{\partial g}{\partial x}\bigg|_{x_j} \cong \partial g^j, \qquad j = 1, 2,..., M. \tag{4.5}$$

By replacing the continuous differential operators in the governing equations by expressions similar to those in Eqs. (4.2)–(4.5), we convert the problem of finding an analytic solution of Eqs. (3.1)–(3.8) to one of finding an approximation to this solution at each point x_j of the mesh $\mathcal{M}$. We seek the solution Z_h^* of the nonlinear system of difference equations

$$F(Z_h^*) = 0. \tag{4.6}$$

In this notation, F is an $(N+1)(M+1)$ vector in which we order the components such that the first $(N+1)$ components correspond to the boundary conditions at $x_0 = 0$. The next $(N+1)(M-1)$ components correspond to the energy and species equations at the interior nodes x_j, $j = 1, 2,..., M-1$. The last $(N+1)$ components correspond to the boundary conditions at $x_M = L$.

For an initial solution estimate Z^0 which is sufficiently close to Z_h^*, the system of nonlinear equations (4.6) can, in principle, be solved by a variety of nonlinear equation methods. A common approach is to apply a version of Newton's method, which we write in the form

$$Z^{n+1} = Z^n - \lambda^n J^{-1}(Z^n)\,F(Z^n). \tag{4.7}$$

Here Z^n denotes the nth solution iterate, λ^n the nth damping parameter $(0 < \lambda \leqslant 1)$, and $J(Z^n) = \partial F(Z^n)/\partial Z$, the $(N+1)(M+1) \times (N+1)(M+1)$ Jacobian matrix. In practice, (4.7) is rewritten in the form

$$J(Z^n)(Z^{n+1} - Z^n) = -\lambda^n F(Z^n), \tag{4.8}$$

where at each iteration a system of linear equations is solved for corrections to the previous solution vector. For problems in which the cost of forming—either analytically or numerically—and then factoring the Jacobian matrix is a significant part of the cost of the total calculation, it is natural to consider applying a modified version of Newton's method in which the Jacobian is re-evaluated only periodically. In determining premixed flame structure, we have found that the numerical evaluation of the Jacobian matrix accounts for 90–95% of the total CPU time for a single Newton step. As a result, we have implemented the modified Newton method

$$J(Z^0)(Z^{n+1} - Z^n) = -F(Z^n), \qquad n = 0, 1, 2,..., \tag{4.9}$$

where the Jacobian is evaluated at the initial solution estimate. The immediate problem one faces when applying the modified method is how to determine whether the sequence of successive modified Newton iterates is converging at a fast enough rate. If the rate of convergence is too slow, we want to revert back to a full Newton method and make use of new Jacobian information and possibly employ a damping strategy. An estimate which enables us to determine an upper bound for the size of the sequence of modified Newton iterates, assuming the Kantorovich hypotheses are satisfied, has been derived in [34]. We apply this result when implementing the method in Eq. (4.9) in the solution of premixed flames. As a result, if in the course of a calculation we determine the size of $\Delta Z^n = Z^{n+1} - Z^n$, $n = 1, 2,...$, to be larger than the value the estimate in [34] predicts, we form a new Jacobian and restart the modified Newton algorithm with a new initial solution estimate given by Z^n.

Although the use of a damped-modified Newton method in the numerical solution of two-point boundary value problems is not unusual, there are several features of our implementation which warrant further discussion.

Assumed Temperature Profile

We note that if the premixed flame problem defined in Eqs. (3.1)–(3.8) is solved with an assumed temperature profile, the energy equation can be replaced by $T = T(x)$, where $T(x)$ is known. One advantage to such a procedure is that if an experimental profile is available, substituting this profile for the energy equation produces a solution of the species Eqs. (3.2), (3.6), (3.8) that is a better representation of the chemistry actually occurring in the flame than if the species equations were solved coupled with the energy equation. The reason is that in actual laboratory applications there can be distributed heat losses (usually radiative) and the temperature predicted by solving the full set of flame equations is often not a good

representation of the temperature profile actually obtained in the laboratory (see Section 5). In addition, in cases where one requires a solution to the full premixed flame equations—predicted temperature and species profiles—the often severe difficulties associated with the convergence of Newton's method can be largely circumvented by first solving the species equations with a specified temperature profile and then solving the full problem with this solution as an initial estimate. The convergence difficulties can be attributed to the exponential nonlinearities occurring in the chemical production terms $\dot{w}_k$, $k = 1, 2, \ldots, N$. The specification of a temperature profile eliminates the exponential nonlinearities in temperature, and the resulting chemical production terms contain nonlinearities that are at most algebraic in the species concentrations.

Upwind Differencing

If a consistent, stable, and hence convergent finite difference method is applied to the flame equations, we anticipate the converged numerical solution Z_h^* to approximate closely the analytic solution at the given mesh points, providing the mesh spacing is *small* enough. For a mesh with coarse grid spacing, however, the converged numerical solution may not accurately resolve the analytic solution at the grid points. As a result, the analytic solution may be a poor initial solution estimate on a coarse grid. To increase the likelihood of convergence of the Newton iteration, it is important that the initial solution estimate on the given grid closely approximate the converged numerical solution on that grid.

The region in which the fuel and the oxidizer react is called the flame zone or burn region. In the flames we have studied, the flame zone is extremely narrow and the temperature and species profiles exhibit sharp gradients in this region. To increase the likelihood of convergence of the Newton iteration, we need an initial solution estimate which is a good approximation to the converged numerical solution on the fine mesh. For the flames we have studied, obtaining an accurate fine-grid initial solution estimate is difficult. Ideally, we would like to be able to specify an initial solution estimate in which an accurate specification of the details of the flame zone is not crucial to the convergence of Newton's method. The ability to obtain such an initial solution estimate is intimately related to how the convective derivatives are approximated and on the size of the initial grid spacing.

We recall that the convective derivatives in Eqs. (3.1)–(3.8) have all been differenced using upwind difference approximations as opposed to second-order centered difference expressions. In the early stages of our work, however, we applied centered difference expressions to the convective derivatives in the governing equations. In a number of problems we were unable to obtain a converged species or a converged energy-species solution. In both cases, Gaussian and cubic S-shaped polynomials were the initial solution estimates (see below). When upwind difference expressions were used for the convective terms, however, we obtained converged species and converged energy-species solutions in almost all the poblems considered. In fact, fewer Newton iterations were required when the problems were solved on an

extremely coarse mesh (4 or 5 subintervals) than on a relative fine mesh (40 to 50 subintervals).

In addition to thermodynamic properties, a fluid is described by transport properties—viscosity, thermal diffusivity, and mass diffusivity. They describe the transport of momentum, heat, and mass, respectively. Since the flow velocities are small, we have neglected viscous effects and hence we are only concerned with the transport of heat and mass. Thermal diffusivity in a flame tends to spread out heat. Mass diffusivity tends to spread out mass. The thermal diffusion rate is given by λ/Cp and the mass diffusion rate is given by ρD_k, $k = 1, 2,..., N$. Due to the truncation error in the upwind difference approximations for the convective terms in Eqs. (3.1)–(3.8), we are, in effect (through first order in h), solving the original flame equations with an extra diffusion term, the size of which is proportional to $\rho u h_j/2$, as opposed to $\rho u(h_{j+1} - h_j)/2$ for centered differences. As a result, the numerical solutions can be broadened depending on the size of $\rho u h_j/2$ or $\rho u(h_{j+1} - h_j)/2$ compared to λ/Cp and ρD_k, $k = 1, 2,..., N$. For problems in which the numerical diffusivity is large compared to the actual diffusion rates, we expect the broadening to be significant. The idea of broadening the solution profiles can be looked upon as making the numerical solution more nearly constant. As a result, one expects to have less difficulty in specifying an initial solution estimate for which the Newton iteration converges than if the high gradient behavior of the numerical solution is preserved. In addition, for a mesh in which the size of adjacent intervals is fairly constant, the quantity $\rho u h_j/2$ can be significantly larger than $\rho u(h_{j+1} - h_j)/2$. As a result, if the solution profiles can be broadened by the use of numerical diffusion, we expect the maximum amount of broadening to be obtained on a coarse mesh with upwind convective derivatives.

Once a solution has been obtained on a coarse mesh, we want to use this solution as an initial solution estimate on a finer mesh with the ultimate goal of being able to resolve accurately the high gradient behavior of the temperature and species profiles in the flame zone. The idea of solving a problem on an initial coarse grid, interpolating the solution to a finer grid, and using the result as an initial estimate to the solution on a finer grid, has been applied by various authors (e.g., [35, 36]). Although most of the applications have centered in the realm of elliptic partial differential equations, ideas along these lines have been used in solving two-point boundary value problems as well (e.g., [18, 37]). Intimately related to this set of ideas is the question of how to determine adaptively the finer mesh.

Adaptive Gridding

We recall from Section 3 that one of the advantages in using an initial value problem method to solve two-point boundary value problems was the adaptive mesh capability of the initial value solver. In such methods, the solution is monitored and the step size appropriately chosen as the integration proceeds. Global finite difference or collocation methods, on the other hand, require that a mesh be determined before the calculation proceeds.

During the last fifteen years, a variety of methods have been developed which attempt to choose optimal grid spacings on which to solve two-point boundary value problems. As Kautsky and Nichols [38] point out, many of these adaptive mesh selection procedures can be interpreted as equidistributing a positive weight function on a given interval. Essentially, one attempts to determine a mesh $\mathcal{M}$ such that the weight function achieves a given constant value over each subinterval. Among the various approaches developed, White [39] has discussed the use of equidistributing the arclength of the solution; Pereyra and Sewell [40] have equidistributed the local truncation error and Pearson [41] has chosen to equalize the change in the discrete solution between consecutive mesh points. Other methods for choosing appropriate meshes for two-point boundary value problems have been investigated, for example, by Russell and Christiansen [42], Ablow and Schecter [43], de Rivas [44], and Denny and Landis [45]. (For an excellent survey on this subject, see Russell [62]).

Following the notation of Kautsky and Nichols, we say that the mesh $\mathcal{M}$ is equidistributed on $[0, L]$ with respect to the nonnegative weight function f and the constant K if

$$\int_{x_j}^{x_{j+1}} f\,dx = K, \qquad j = 0, 1,..., M-1. \tag{4.10}$$

Similarly, $\mathcal{M}$ is called sub-equidistributing on $[0, L]$ with respect to f and K if

$$\int_{x_j}^{x_{j+1}} f\,dx \leqslant K, \qquad j = 0, 1,..., M-1. \tag{4.11}$$

For convenience, we shall refer to f as being equidistributed in (4.10) and sub-equidistributed in (4.11).

Our experience with the various equidistribution techniques indicates that while they may all be viable mesh selection procedures in theory, some are to be preferred over others in practice. We have found that, as the size of a two-point boundary value problem increases and/or the problem becomes more nonlinear, the selection of a mesh by attempting to equidistribute a nonnegative weight function over a given interval through an implicit change of variables becomes less practical than by attempting to sub-equidistribute a nonnegative weight function over a given interval by explicitly using the numerical solution on the given grid. For example, we have applied arclength and boundary layer coordinate transformations to several test problems. Although these methods worked for a number of simple scalar problems, as the size and the degree of complexity of the problems grew, we needed better and better starting estimates to obtain converged numerical solutions. In fact, we could never generate a converged numerical solution to the premixed flame equations using the arclength transformation, even when the problem was first solved on nonuniform grids with 25 to 50 grid points and then this solution became the initial solution estimate to the problem with the arclength transformation *turned on*—a two-pass solution method.

The approach we have chosen to determine an adaptive grid for the premixed flame problem is similar to the method used by Pearson [41] in solving scalar boundary layer problems. We attempt to sub-equidistribute the difference in the components of the discrete solution and the difference in the gradient of the components of the discrete solution between adjacent mesh points. Upon denoting the $(N+1)$ vector S such that

$$S^t = [T, Y_1, Y_2, \ldots, Y_N], \tag{4.12}$$

we seek to obtain a mesh $\mathscr{M}$ such that

$$\int_{x_j}^{x_{j+1}} \left| \frac{dS_i}{dx} \right| dx \leqslant \delta(\max_{0 \leqslant x \leqslant L} |S_i|), \qquad j = 0, 1, \ldots, M-1, \quad i = 1, 2, \ldots, N+1, \tag{4.13}$$

and

$$\int_{x_j}^{x_{j+1}} \left| \frac{d^2 S_i}{dx^2} \right| dx \leqslant \gamma \left(\max_{0 \leqslant x \leqslant L} \left| \frac{dS_i}{dx} \right| \right), \qquad j = 1, 2, \ldots, M-1, \quad i = 1, 2, \ldots, N+1, \tag{4.14}$$

where δ and γ are small numbers less than one and the values of $\max |S_i|$ and $\max |dS_i/dx|$ are obtained from a converged numerical solution on a previously determined mesh.

A potential disadvantage of such a procedure is the formation of a mesh which may not be smoothly varying. For example, the ratio of consecutive mesh intervals may differ by several orders of magnitude. This can affect the convergence properties as well as the accuracy of the method. As a result, we impose the added constraint that the mesh produced by employing the restrictions in Eq. (4.13) and (4.14) be locally bounded, i.e., the ratio of adjacent mesh intervals must be bounded above and below by constants. We require that

$$1/C \leqslant h_j/h_{j-1} \leqslant C, \qquad j = 2, 3, \ldots, M, \tag{4.15}$$

where C is a constant $\geqslant 1$. Such a *buffering* of the mesh tends to smooth out rapid changes in the size of the mesh intervals.

In our adaptive mesh algorithm, we first solve the flame equations on a coarse mesh (4 to 5 subintervals). The maximum values of $|S_i|$ and $|dS_i/dx|$ are then obtained. We next test the inequalities in Eqs. (4.13) and (4.14) for each of the $N+1$ components (or N if we are only solving the species equations) of S at the nodes of the coarse mesh. If either of the inequalities is not satisfied, a grid point is inserted at the midpoint of the interval in question. Once a new mesh has been obtained, we check to see whether it is locally bounded. If it is not, a grid point is inserted at the midpoint of the intervals in which the inequality in Eq. (4.15) is not satisfied. The previously converged numerical solution is interpolated onto this new mesh and the result serves as an initial solution estimate for Newton's method on this finer grid.

The flame equations are solved on the new mesh and the process continues until the inequalities in Eqs. (4.13)–(4.15) are satisfied.

We remark that if we had refined the mesh by using only the inequality in Eq. (4.13), we would have been able to resolve high gradient regions but we would have had difficulty in resolving the wings and the peaks of spikelike solution profiles. These are typically regions in which the solution components exhibit high curvature. The test in Eq. (4.14) is designed to refine the mesh in these regions.

Computational Considerations

Before concluding this section, it is worthwhile to discuss a few points concerning the numerical implementation of the method.

Numerical Jacobian

With the difference approximations we have chosen to employ, the energy and species equations at an interior node j only contain references to the temperature and species at nodes $j-1$, j, and $j+1$. (The boundary conditions contain references to only one adjacent node). As a result, the Jacobian matrix in Eq. (4.8) can be written in block tridiagonal form. Although we considered evaluating the Jacobian analytically, we found that in problems characterized by complicated transport coefficients and complex chemistry, such a procedure was not very efficient. As a result, we evaluate all the Jacobians by a numerical finite difference procedure. If we denote the dependent solution vector by Z, then the ijth element of the Jacobian matrix $J_{ij}(Z) = \partial F_i/\partial Z_j$ can be approximated by the relation

$$J_{ij}(Z) = \frac{\partial F_i}{\partial Z_j} = \frac{F_i(Z + \delta Z_j I_j) - F_i(Z)}{\delta Z_j}, \tag{4.16}$$

where I_j is the jth column of the identity matrix and δZ_j is a small perturbation of the jth component of the vector Z. For our problems, we let

$$\delta Z_j = \alpha Z_j + \beta, \tag{4.17}$$

where α and β are typically both taken to be the square root of the unit round-off error for the machine on which we are computing. As we mentioned earlier, the cost of evaluating the Jacobian and hence the function F is very high. As a result, we would like to minimize the total number of function evaluations required to estimate the Jacobian matrix. Curtis, Powell, and Reid [46] have discussed such a method. The procedure they outline takes advantage of the zero-nonzero structure of the Jacobian. For our problem, we can compute several columns of the Jacobian simultaneously by first evaluating F at some vector Z. We then perturb every $3N$th element of Z (as in Eq. (4.17)) beginning with the first. The function is evaluated at this new point and the appropriate difference quotient is formed. The procedure is repeated beginning with the second element of Z and the cycle is continued until the first $3N$ elements of Z have been perturbed. In particular, if we denote the kth column

of J by J_k, then for a fixed i, $i = 1, 2,..., 3N$, the columns $i + 3Nj, j = 0, 1,..., \tilde{M}_i$, can be calculated by evaluating

$$J_{i+3Nj} = \left[F\left(Z + \sum_{k=0}^{\tilde{M}_i} \delta Z_{i+3Nk} I_{i+3Nk} \right) - F(Z) \right] \Big/ \delta Z_{i+3Nj}, \tag{4.18}$$

where $\tilde{M}_i$ is the largest integer such that $1 + 3N\tilde{M}_i \leqslant MN$. As a result, we can form the entire numerical Jacobian in $3N + 1$ vector function evaluations. Once the Jacobian is formed, a block tridiagonal set of linear equations must be solved. We use the block tridiagonal routines DECBT and SOLBT written by Hindmarsh [47].

Scaling

In problems of interest, the maximum values of the temperature and the mass fractions of the species under investigation typically range over several orders of magnitude. In particular, there are problems in which the ratio of $\max_{0 \leqslant x \leqslant L} T / \min_{1 \leqslant i \leqslant N}(\max_{0 \leqslant x \leqslant L} Y_i)$ may be larger than 10^{10}. Problems of this type are said to be poorly scaled. This can result in an unsuitable choice of pivots in the Newton equations (4.8) or (4.9) with possible disastrous effects on the accuracy of the computed solutions. We have chosen to scale the mass fractions of the species under investigation by the maximum value they can attain in a given calculation. The new mass fractions $\tilde{Y}_i$ are given by

$$\tilde{Y}_i = Y_i / Y_{i,\max}, \qquad i = 1, 2,..., N, \tag{4.19}$$

Damping and Convergence

The choice of the damping parameter λ^i to ensure monotonic convergence of the full Newton iteration (4.8) has been studied in depth by Deuflhard [48]. We have implemented a variation of his method for nonsingular Jacobians. As it turns out, however, with the exception of the first couple of iterations on the initial mesh, we almost always take full Newton steps on each refined grid. We terminate the Newton iteration when

$$\|\Delta Z^{n+1}\|_2 = \|Z^{n+1} - Z^n\|_2 \leqslant \mathrm{TOL}, \qquad n = 0, 1, 2,..., \tag{4.20}$$

where we typically take $\mathrm{TOL} \leqslant 10^{-5}$.

Initial Estimates

Of critical importance to the success of the boundary value method we outlined above is the ability to obtain an initial solution estimate which lies in the domain of convergence of Newton's method. Although we have already discussed the use of one-sided difference expressions and coarse mesh Newton iterations in increasing the

likelihood of obtaining a converged numerical solution for a given starting estimate, we only briefly mentioned the actual choice of our initial solution profiles—*S*-shaped and Gaussian. To generate these profiles we require an estimate of the center and the width of the flame zone. The minor species (intermediates) are then fitted by Gaussian curves which are centered at the middle of the flame zone and which are equal to 10% of the specified peak values at the boundaries of the flame zone. The major species (reactants and products), on the other hand, are given specified values both before and after the flame zone. Inside this region they are fitted to cubic polynomials such that the profiles have zero slope and interpolate the input values at the boundaries of the region.

Constitutive Relations

In calculating the binary diffusion coefficients, the single component conductivities, and the thermal diffusion coefficients, collision integrals must be evaluated. Rather than perform a numerical quadrature, we have approximated the necessary collision integrals by polynomial fits to the tabulated data of Monchick and Mason [49]. The degree of the polynomials was chosen to guarantee at most a 1% deviation from the tabulated data in [49]. Thermodynamic properties (heat capacities, entropies, and enthalpies) are computed from fits of the JANNAF data [50] used in the NASA chemical equilibrium code [51]. Stockmayer potentials are used throughout in evaluating transport properties, and the potential parameters are compiled from various tabulated sources (e.g., [29]). In our computations, all the chemical production rate terms, thermodynamic properties, and equation of state variables are evaluated using CHEMKIN, the chemical kinetics code package written by Kee *et al.* [52].

5. Numerical Results

This section discusses the results obtained by applying our method to several laboratory flames.

Test Flames

We have applied the boundary value method to a variety of laboratory flames. In the remainder of this section, we discuss the results of our calculations for premixed hydrogen-oxygen, methane-oxygen, and acetylene-oxygen flames, and we compare the results of our calculations with experimental data. In evaluating our results, we must consider several factors: First, how well the governing equations model the physical system we are investigating; second, the accuracy with which the numerical method solves the governing equations; and finally, how well the chemical reaction mechanism describes the evolution of the fuel/oxidizer system and the formation of the resulting intermediates and products. The form of the flame equations we are using is fairly standard. Solving the equations for a hydrogen-air test system by

several numerical methods has produced results which compare favorably with experimental data [53]. In addition, we have tested the boundary value method discussed above on a variety of two-point boundary test problems (e.g., [16, 54]). In the cases considered, we have obtained good agreement between our numerical solution and the solutions obtained by other two-point boundary value solution methods. The reaction mechanism, however, is the largest source of uncertainty in numerical flame modelling. Many of the reaction paths, rate constants, and activation energies are not accurately known. As a result, we expect that our results should agree well with experiment only where the reaction paths are well understood and the rate constants are well known. The reaction mechanisms (see Appendix) used in the calculations have been included for completeness. They are all actively being studied and are not the definitive reaction set for the corresponding fuel/oxidizer systems. All the calculations were performed on the CRAY-I computer at Sandia National Laboratories, Livermore.

Hydrogen-Oxygen Flame (H_2/O_2)

Eberius *et al.* [22] have experimentally studied a rich, low-pressure, hydrogen-oxygen flame. Table I lists the fuel/oxidizer content of the unburnt gases, the flow velocity, and the pressure. The species considered are given in Table II, and the reaction mechanism used in the calculation is given in Table VII in the Appendix.

In an earlier section, we discussed solving the species equations with a specified temperature profile. We mentioned that if an experimental temperature profile was available, substituting this profile for the energy equation produces a solution of species Eqs. (3.2), (3.6), and (3.8), which is often a better representation of the chemistry actually occurring in the flame than if the species equations were solved

TABLE I

H_2/O_2 Flame Parameters

Unburnt mixture	75 mole % H_2/25 mole % O_2
Flow velocity (u)	178 cm/sec
Pressure (p)	10.6 torr

TABLE II

Species for H_2/O_2 Flame

H_2	O_2
H	O
OH	HO_2
H_2O_2	H_2O

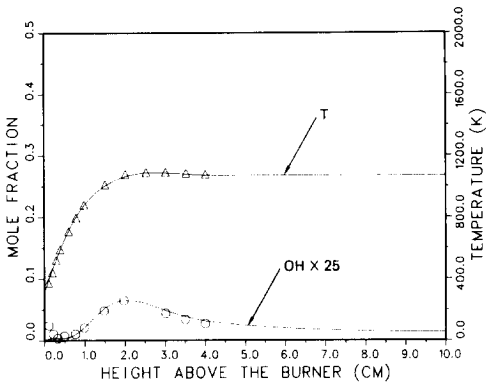

FIG. 2. Experimental (O) and calculated (—) OH profiles for a hydrogen-oxygen flame studied experimentally by Eberius *et al.* [22]. The calculation was performed by replacing the energy equation with an extension (—) of experimental temperature results (△).

coupled with the energy equation. We attributed this to the fact that in actual laboratory applications there are usually distributed heat losses and the temperature predicted by solving the full set of flame equations is not always a good representation of the temperature actually obtained in the laboratory. To illustrate these ideas, we consider the OH and temperature profiles for the hydrogen-oxygen flame we are investigating.

In Fig. 2 we show the experimental and calculated (—) OH profiles for the hydrogen-oxygen system. We also include the experimental temperature data. The line connecting the temperature points was obtained by a least-squares fit to the data. The line has been extended past 4 cm such that a zero temperature gradient is obtained as we approach 10 cm. The predicted OH profile agrees well with the data.

In Fig. 3, however, we show the solution in which the energy equation is solved

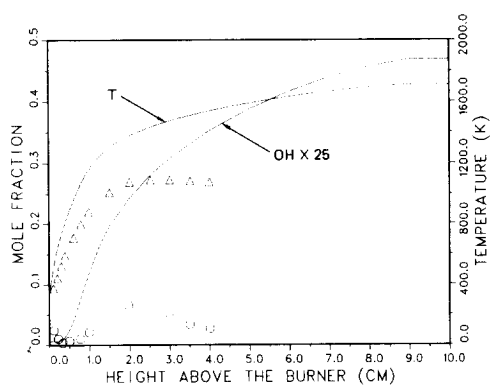

FIG. 3. Experimental (O, △) and calculated (—) OH and temperature profiles for a hydrogen-oxygen flame studied experimentally by Eberius *et al.* [22]. The calculation was performed by solving the energy and species equations together.

coupled with the species equations. The initial temperature profile is just the extended experimental temperature profile linearly interpolated to the initial coarse gird. In this case, the calculated OH concentration and the calculated temperature profile (—) are much higher than observed experimentally. This calculation illustrates two points. First, use of an experimental temperature profile instead of a solution to the energy equation can allow physically realistic chemical kinetic modelling of the flame; and second, the solution method presented above allows one to obtain a solution to the energy equation even when the initial guess is bad (compare Figs. 2 and 3).

Both calculations were performed using a 10 cm interval with an initial grid consisting of five equally spaced subintervals. The calculation with the experimental temperature profile required 45 adaptively placed grid points in order to obtain three significant figures of accuracy in the numerical solution. The calculation in which the energy and species equations were solved together required 34 points to achieve the same degree of accuracy. A large number of the grid points for the two calculations were located in the flame zone, which for our purposes is defined as the region in which

$$T_b + 0.1\Delta T_b \leqslant T \leqslant T_b + 0.9\Delta T_b, \tag{5.6}$$

where

$$\Delta T_b = T_{\max} - T_b, \tag{5.7}$$

and $T_{\max}$ denotes the peak temperature of the flame under investigation.

For the first calculation, 22 of the 45 grid points were in the flame zone. The ratio of the largest to the smallest mesh interval—$h_{\max}/h_{\min}$—was 64 while the ratio of the length of the integration inverval to the smallest mesh interval—$L/h_{\min}$—was 640. In the second calculation, 25 of the 34 grid points were in the flame zone with $h_{\max}/h_{\min} = 128$ and $L/h_{\min} = 1280$. The grids for both calculations were refined a total of eight times after a converged numerical solution was obtained on the coarsest grid. The calculations were performed without thermal diffusion and the cross-sectional area of the flame was taken as constant. The first calculation took 20 seconds of CPU time while the second took 33.

Methane-Oxygen Flame (CH_4/O_2)

Peeters and Mahnen [55] have experimentally studied a lean, low-pressure methane-oxygen flame. Table III lists the fuel/oxidizer content of the unburnt gases,

TABLE III

CH_4/O_2 Flame Parameters

Unburnt mixture	9.5 mole % CH_4/90.5 mole % O_2
Flow velocity (u)	67 cm/sec
Pressure (p)	40 torr

TABLE IV

Species for CH_4/O_2 Flame

H_2	O_2
H	O
OH	HO_2
H_2O_2	HCO
CH_2O	CO
CO_2	CH_4
CH_3	

the flow velocity, and the pressure. The species considered are given in Table IV and the reaction mechanism used in the calculation is identical to the one used by Tsatsaronis [61] in his work on methane-oxygen flames. It is given in Table VIII in the Appendix.

Section 4 discussed the use of upwind differencing for the convective derivatives in Eqs. (3.1)–(3.8). We noted that this type of difference approximation could significantly broaden the numerical solution profiles depending upon the size of $\rho u h_j/2$, $j = 1, 2, \ldots, M$, compared to λ/C_p and/or ρD_k, $k = 1, 2, \ldots, M$. In addition, we anticipated the broadening to be greater on a coarse mesh than on a fine one. In Fig. 4 are shown a family of curves representing the H_2 solution profile for the methane-oxygen system on successively finer grids. The solution on the coarsest grid (five subintervals) does not resolve the height of the peak and the profile is broadened due to numerical diffusion (compare the location of the peaks on the coarse and the fine grids). As the grid is refined, however, we secure better and better resolution of the H_2 peak, until a highly resolved solution is obtained. In Fig. 5 we show the results of a similar calculation for the CO profile. On a grid with 65 subintervals, excellent resolution of the solution profile is obtained.

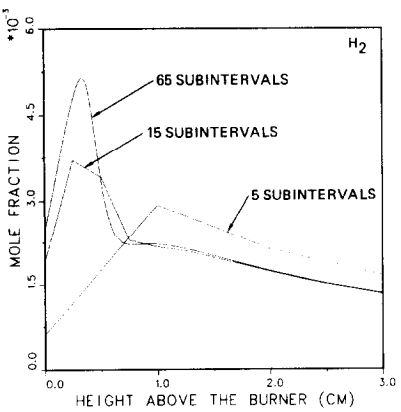

FIG. 4. Calculated H_2 profiles for a methane-oxygen flame studied experimentally by Peeters and Mahnen [53]. The curves represent the numerical solution on successively finer grids.

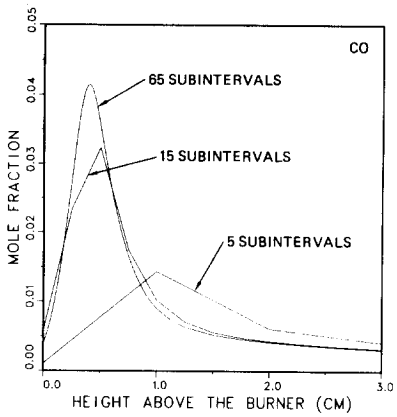

FIG. 5. Calculated CO profiles for a methane-oxygen flame studied experimentally by Peeters and Mahnen [53]. The curves represent the numerical solution on successively finer grids.

In Figs. 6–8, we compare the results of our calculation (solid lines) with the experimental profiles of Peeters and Mahnen. There is good agreement between the calculated and experimental profiles for CH_4, O_2, CO_2, H_2O, and CO. The agreement between the calculated and the experimental profiles for H and OH is not quite as good, but they differ by at most a fraction of a mole percent. We anticipate that with further study of the kinetics mechanism for this flame, we should be able to secure better agreement between the calculated and the experimental profiles for these species.

The calculation was performed by replacing the energy equation with the experimental temperature profile extended out to 5 cm, much as was done in the hydrogen-oxygen system. A solution was sought on an interval of 5 cm with an initial

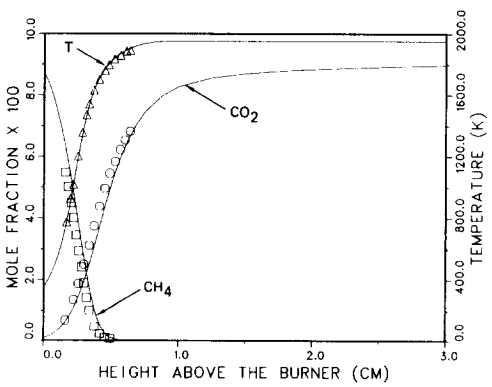

FIG. 6. Experimental (□, ○) and calculated (—) profiles of CH_4 and CO_2 for a methane-oxygen flame studied experimentally by Peeters and Mahnen [53]. The calculation was performed by replacing the energy equation with an extension (—) of experimental temperature results (△).

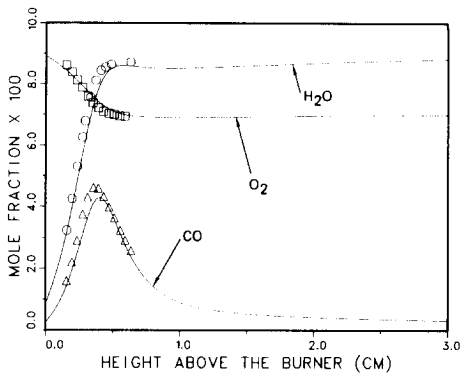

FIG. 7. Experimental (□, ○, △) and calculated (—) profiles of O_2, H_2O, and CO for a methane-oxygen flame studied experimentally by Peeters and Mahnen [53].

grid consisting of five equally spaced subintervals. A total of 45 adaptively placed grid points were required to obtain three significant figures of accuracy; 24 of these points were in the flame zone. The value of h_{max}/h_{min} was 64 and L/h_{min} was 160. Seven mesh refinements were performed. The calculation took 41 seconds of CPU time and was performed without thermal diffusion and with a constant cross-sectional area.

Acetylene-Oxygen Flame (C_2H_2/O_2)

The final flame we want to discuss is a lean, low-pressure acetylene-oxygen flame studied experimentally by Eberius *et al.* [56]. The content of the unburnt gases, the flow velocity, and the pressure are listed in Table V. The species considered are given in Table VI. The reaction mechanism used in the calculation is listed in Table IX in the Appendix.

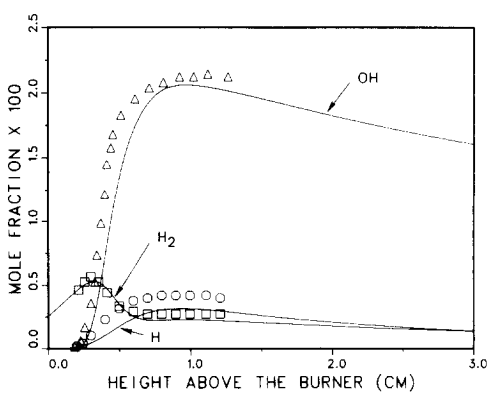

FIG. 8. Experimental (△, □, ○) and calculated (—) profiles of OH, H_2, and H for a methane-oxygen flame studied experimentally by Peeters and Mahnen [53].

TABLE V

C_2H_2/O_2 Flame Parameters

Unburnt mixture	3.0 mole % C_2H_2/97.0 mole % O_2
Flow velocity (u)	78 cm/sec
Pressure (p)	10.6 torr

TABLE VI

Species for C_2H_2/O_2 Flame

H_2	O_2	CH_2CO	CO
H	O	CO_2	C_2H_2
OH	HO_2	C_2H	CH_2
H_2O_2	H_2O	CH	CH_3
HCO	CH_2O	HCCO	C_2H_3

In Section 4, we mentioned that in recent years a variety of methods have been used to determine adaptive grids for two-point boundary value problems. The method we have implemented sub-equidistributes the difference in the components and the difference in the gradient of the components of the discrete solution between consecutive grid points. To illustrate the importance of adaptively placing grid points in the flame zone to the accuracy and efficiency of the flame calculation, we have performed several calculations for the acetylene-oxygen system using equally spaced grids and adaptively determined grids. In Fig. 9, we illustrate the molecular hydrogen profile for a series of calculations for 20, 40, 80, and 160 equally spaced points. We

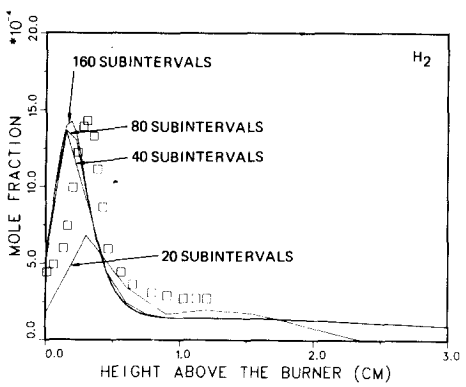

FIG. 9. Experimental (□) and calculated (—) H_2 profiles for an acetylene-oxygen flame studied experimentally by Eberius *et al.* [56]. The curves represent the numerical solution on 20, 40, 80, and 160 equally spaced subintervals.

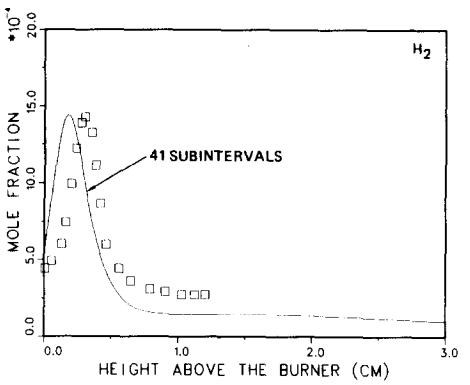

FIG. 10. Experimental (□) and calculated (—) H_2 profile for an acetylene-oxygen flame studied experimentally by Eberius *et al.* [56]. The curve represents the numerical solution in which 41 adaptively placed points were used.

include the experimental data for reference. We secure not only a much smoother solution, but one which agrees better with the experimental data as we go to a finer and finer grid.

In Fig. 10, we plot the molecular hydrogen profile for a calculation in which 41 adaptively placed points were used to obtain three significant figures of accuracy in the solution. As one expects, the adaptive calculation secures a highly resolved species profile with far fewer points than is required using an equally spaced grid. In Figs. 11 and 12, we compare the results of the adaptive calculation with the experimental profiles of Eberius *et al.* [56]. The calculation and experiment agree well, and we anticipate that with further study of the reaction mechanism we should be able to secure better agreement between the calculated and the experimental profiles.

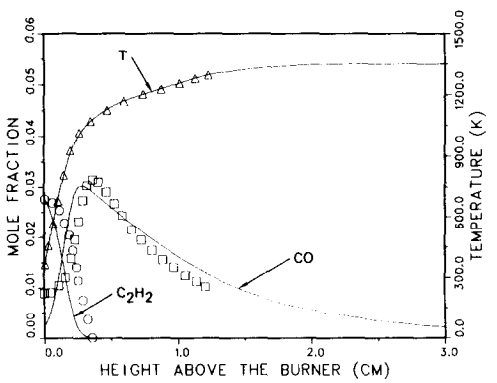

FIG. 11. Experimental (○, □) and calculated (—) profiles of C_2H_2 and CO for an acetylene-oxygen flame studied experimentally by Eberius *et al.* [56]. The calculation was performed by replacing the energy equation with an extension (—) of experimental temperature results (△).

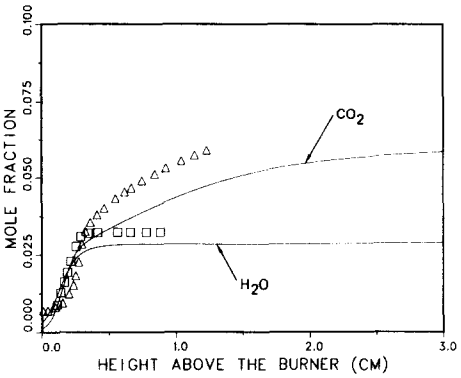

FIG. 12. Experimental (□, △) and calculated (—) profiles of H_2O and CO_2 profiles for an acetylene-oxygen flame studied experimentally by Eberius *et al.* [56].

The adaptive and equally spaced calculations were performed by replacing the energy equation with the experimental temperature profile extended out to 6 cm in a manner similar to that used in the hydrogen and methane systems. For both the adaptive and equally spaced calculations, a solution was sought on an interval of 6 cm with an initial grid consisting of ten equally spaced subintervals. In the adaptive calculation, 19 of the 41 adaptively placed grid points were in the flame zone. The value of h_{max}/h_{min} was 64 and L/h_{min} was 640. The calculation took 276 second of CPU time and was performed with thermal diffusion and a constant cross-sectional area.

To generate the equally spaced solution on 160 subintervals, we first obtained a solution on the initial ten subinterval grid. The number of mesh intervals was doubled and a solution was obtained on the new grid with 20 subintervals. The process was repeated for 40, 80, and 160 subintervals. The equally spaced calculation with 160 subintervals took 585 seconds of CPU time and was performed with thermal diffusion and a constant cross-sectional area.

Discussion

The efficiency of a numerical method is, to a large extent, based upon the CPU time required to solve a given problem to a specified degree of accuracy. It is difficult, however, to make an accurate comparison of the efficiency of our steady state method and existing time-dependent solution methods. Differences in the complexity of the governing equations combined with differences in the transport algorithms and differences in the initialization and termination criteria make it difficult to perform such a comparison. The situation is complicated even more since a number of computers have been used in the various time-dependent calculations. Ideally, a standard test problem with a standard set of governing equations and a standard set of initialization and termination criteria should be used to test the various solution methods on a specified computer. While such a study is needed, it is

and illustrate why the steady state method we have developed is more efficient than a class of time-dependent methods for solving premixed flame problems.

In solving the premixed flame equations by time-dependent methods, the original nonlinear two-point boundary value problem is converted into a nonlinear parabolic mixed initial-boundary value problem. This is accomplished by adding a $\partial(\cdot)/\partial t$ term to Eqs. (3.2) and (3.3) (initial conditions must also be specified). By discretizing the resulting equations and boundary conditions, much as was done in obtaining Eqs. (4.6), we can write the flame equations in the semi-discrete form

$$\frac{\partial Z_h}{\partial t} = F(Z_h), \tag{5.8}$$

with appropriate initial conditions. To solve this system of initial value problems, we advance the numerical solution from the initial point $t_0 = 0$ through time levels $0 = t_0 < t_1 < t_2 < \cdots < t_J = \mathscr{T}$, for some finite time $\mathscr{T}$. If for a continuous mapping $g: [0, \mathscr{T}] \to \mathscr{L}^2(0, L)$, we define $g^n = g(t_n)$, $n = 0, 1, 2, \ldots, J$, then an approximation of $\partial Z_h/\partial t$ at $t = t_{n+1}$ can be written in the form

$$\left.\frac{\partial Z_h}{\partial t}\right|_{t=t_{n+1}} = (Z_h^{n+1} - Z_h^n)/\tau_{n+1}, \qquad n \geqslant 0, \tag{5.9}$$

where the time step $\tau_{n+1} = t_{n+1} - t_n$. If we incorporate Eq. (5.9) in Eq. (5.8) and evaluate F at Z_h^{n+1}, we obtain the implicit Euler formulation of the time-dependent flame equations

$$\mathscr{F}(Z_h^{n+1}) = F(Z_h^{n+1}) - ((Z_h^{n+1} - Z_h^n)/\tau_{n+1}) = 0, \qquad n \geqslant 0. \tag{5.10}$$

At each time level, therefore, we must solve a system of nonlinear equations. It turns out that many of the time-dependent solution methods employ some form of implicit time differencing (e.g., [6, 7, 10, 12, 57]). For each of these methods, a system of nonlinear equations must also be solved at each time level. For a sufficiently good starting estimate, the system of nonlinear equations in (5.10) can be solved by Newton's method. If we omit the subscript h, we have

$$(J(Z_k^{n+1}) - (I/\tau_{n+1}))(Z_{k+1}^{n+1} - Z_k^{n+1}) = -\mathscr{F}(Z_k^{n+1}), \qquad n \geqslant 0, \quad k = 0, 1, 2, \ldots, \tag{5.11}$$

where I is the identity matrix. We note that, in order to solve Eqs. (5.11), we must still form the steady state Jacobian matrix, J. The converged solution at the nth time step, however, provides an excellent starting guess to the solution at the $(n+1)$st time level. The work per time step is similar to that for a steady state Newton iteration, but the timelike continuation of the numerical solution implies that the iteration strategy in Eqs. (5.10) and (5.11) will, in general, be less sensitive to the initial starting estimate than if Newton's method were applied to Eq. (4.6). This ability to converge to a steady state solution from a starting estimate which may not lie in the domain of convergence of Newton's method for Eq. (4.6), is the primary

reason for the widespread use of implicit time-dependent methods in solving premixed flame problems. In addition to the adaptive mesh capability we have developed, a major result of our work has been the ability to reduce the sensitivity of the Newton iteration to the initial starting estimate so that we can deal directly with Eq. (4.6). As a result, we can reliably solve the premixed flame equations without resorting to a time relaxation procedure.

By comparing the number of iterations required to reach a steady state solution for the time-dependent method discussed above with the number of Newton iterations used in our steady state method, we can get a reasonable estimate (independent of the problem) of the relative efficiency of the two methods. In typical premixed flame calculations 200 to 500 time steps with two or three Newton iterations per step is not unusual [58, 59]. In our steady state method, we average about six Newton iterations per grid with five to nine grids used in a typical calculation. Based upon these numbers it is reasonable to expect the steady state method to be faster by about a factor of 7 to 50 than the time-dependent method. In an efficient implementation of the time-dependent method, however, one does not recalculate the Jacobian at every Newton iteration, and a Jacobian is often used for several consecutive time steps. On the other hand, most of our steady state Newton iterations are performed on grids consisting of only a few grid points, and we also do not re-evaluate the Jacobian after every Newton iteration. We estimate that a factor of 5 to 10 is more realistic.

The above analysis was designed to give a rough indication of the efficiency of our steady state method and a class of implicit time-dependent methods. We realize that time-dependent marching methods (e.g., [3, 8]) and time-dependent implicit methods that employ high order time differencing schemes [10] have also been used to calculate premixed flame structure. The above analysis does not apply directly to these methods. We point out, however, that, for stability reasons, much smaller time steps must be taken in explicit time-dependent calculations as opposed to implicit methods, though the cost of the step is less. In addition, although the higher order implicit time differencing methods may require fewer steps to reach a steady state, the cost per step is greater than the implicit Euler method discussed above.

6. Remarks

The diffulties associated with obtaining *good* starting estimates and with being able to resolve the temperature and species profiles accurately in high gradient and high curvature regions have limited the use of steady state methods in calculating premixed flame structure. As a result, most of the papers in the literature which are concerned with the numerical solution of the premixed flame equations employ some type of time-dependent method. The slow relaxation of time-dependent methods to steady state can, however, make parameter studies employing complicated nonlinear transport properties and chemical kinetics extremely time consuming. Steady state methods, on the other hand, have the potential of solving the flame equations in much less time than time dependent methods.

In this paper, we have developed a steady state numerical method which reduces the sensitivity of the flame equations to the initial solution estimate, and we have also shown how to place grid points adaptively in regions where the dependent solution components are undergoing rapid change. The method employs a global finite difference technique in which the nonlinear difference equations are solved by a damped-modified Newton method. We use upwind difference expressions for the convective derivatives and an assumed temperature profile to help generate a converged numerical solution on an initial coarse grid. Mesh points are inserted in regions where the solution components and their gradients vary most rapidly. We have applied the method to the calculation of the temperature and/or species profiles for several laboratory flames, and we have obtained good agreement with experiment.

APPENDIX

In this section we tabulate the reaction mechanisms used in the three test calculations.

TABLE VII

H_2/O_2 Reaction Mechanism [57, 60]

j	Reaction	A_j^f	β_j^f	E_j^f
1	$H_2 + O_2 \leftrightarrows 2OH$	1.7×10^{13}	0.0	47780.0
2	$OH + H_2 \leftrightarrows H_2O + H$	2.2×10^{13}	0.0	5140.0
3	$H + O_2 \leftrightarrows OH + O$	7.19×10^{16}	−0.861	16523.0
4	$O + H_2 \leftrightarrows OH + H$	1.8×10^{10}	1.0	8826.0
5	$H + O_2 + M \leftrightarrows HO_2 + M$ H_2 enhanced by 3.0 H_2O enhanced by 15.0	2.0×10^{15}	0.0	−1000.0
6	$OH + HO_2 \leftrightarrows H_2O + O_2$	5.0×10^{13}	0.0	1000.0
7	$H + HO_2 \leftrightarrows OH + OH$	2.5×10^{14}	0.0	1900.0
8	$O + HO_2 \leftrightarrows O_2 + OH$	4.8×10^{13}	0.0	1000.0
9	$2OH \leftrightarrows O + H_2O$	6.0×10^{8}	1.3	0.0
10	$H_2 + M \leftrightarrows H + H + M$ H_2O enhanced by 6.0 H enhanced by 20.0 H_2 enhanced by 3.0	2.23×10^{12}	0.5	92600.0
11	$O_2 + M \leftrightarrows 2O + M$	1.85×10^{11}	0.5	95560.0
12	$H + OH + M \leftrightarrows H_2O + M$ H_2O enhanced by 19.0	7.5×10^{23}	−2.6	0.0
13	$H + HO_2 \leftrightarrows H_2 + O_2$	2.5×10^{13}	0.0	700.0
14	$HO_2 + HO_2 \leftrightarrows H_2O_2 + O_2$	2.0×10^{12}	0.0	0.0
15	$H_2O_2 + M \leftrightarrows OH + OH + M$	1.3×10^{17}	0.0	45500.0
16	$H_2O_2 + H \leftrightarrows HO_2 + H_2$	1.6×10^{12}	0.0	3800.0
17	$H_2O_2 + OH \leftrightarrows H_2O + HO_2$	1.0×10^{13}	0.0	1800.0

Note. $k_j^f = A_j^f T^{\beta_j^f} e^{-E_j^f/RT}$ (units are moles, cm^3, sec).

TABLE VIII

CH_4/O_2 Reaction Mechanism [61]

j	Reaction	A_j^f	β_j^f	E_j^f
1	$CH_4 + H \leftrightarrows CH_3 + H_2$	2.24×10^4	3.0	8800.0
2	$CH_4 + OH \leftrightarrows CH_3 + H_2O$	2.2×10^{13}	0.0	5000.0
3	$CH_4 + O \leftrightarrows CH_3 + OH$	1.26×10^{14}	0.0	12000.0
4	$CH_3 + O \leftrightarrows CH_2O + H$	2.0×10^{14}	0.0	2000.0
5	$CH_3 + O_2 \leftrightarrows CH_2O + OH$	1.0×10^{11}	0.0	10000.0
6	$CH_2O + H \leftrightarrows HCO + H_2$	1.25×10^{10}	1.0	3200.0
7	$CH_2O + OH \leftrightarrows HCO + H_2O$	4.8×10^{13}	0.0	0.0
8	$CH_2O + O \leftrightarrows HCO + OH$	5.0×10^{13}	0.0	4600.0
9	$CH_2O + M \leftrightarrows CO + H_2 + M$	2.0×10^{16}	0.0	38000.0
10	$HCO + H \leftrightarrows CO + H_2$	2.0×10^{14}	0.0	0.0
11	$HCO + OH \leftrightarrows CO + H_2O$	1.0×10^{14}	0.0	0.0
12	$HCO + O \leftrightarrows CO + OH$	3.0×10^{11}	1.0	500.0
13	$HCO + O_2 \leftrightarrows CO + HO_2$	3.0×10^{13}	0.0	0.0
14	$HCO + M \leftrightarrows CO + H + M$	5.0×10^{12}	0.0	19200.0
15	$CO + OH \leftrightarrows CO_2 + H$	2.5×10^{12}	0.0	5800.0
16	$CO + O + M \leftrightarrows CO_2 + M$	3.6×10^{18}	−1.0	2600.0
17	$OH + H_2 \leftrightarrows H_2O + H$	2.2×10^{13}	0.0	5200.0
18	$H + O_2 \leftrightarrows OH + O$	2.2×10^{14}	0.0	16800.0
19	$O + H_2 \leftrightarrows OH + H$	1.8×10^{10}	1.0	9000.0
20	$H + O_2 + M \leftrightarrows HO_2 + M$	1.4×10^{16}	0.0	−1000.0
21	$HO_2 + H \leftrightarrows OH + OH$	2.0×10^{14}	0.0	2000.0
22	$HO_2 + H \leftrightarrows H_2O + O$	5.0×10^{13}	0.0	1000.0
23	$HO_2 + H \leftrightarrows H_2 + O_2$	6.0×10^{13}	0.0	2000.0
24	$HO_2 + OH \leftrightarrows H_2O + O_2$	4.0×10^{13}	0.0	0.0
25	$HO_2 + O \leftrightarrows OH + O_2$	6.0×10^{13}	0.0	0.0
26	$H + OH + M \leftrightarrows H_2O + M$	2.3×10^{22}	−2.0	0.0
27	$H + O + M \leftrightarrows OH + M$	6.2×10^{16}	−0.6	0.0
28	$OH + OH \leftrightarrows H_2O + O$	6.3×10^{12}	0.0	1100.0
29	$H + H + M \leftrightarrows H_2 + M$	2.0×10^{19}	−1.0	0.0

Note. $k_j^f = A_j^f T^{\beta_j^f} e^{-E_j^f/RT}$ (units are moles, cm^3, sec).

TABLE IX

C_2H_2/O_2 Reaction Mechanism [60]

j	Reaction	A_j^f	β_j^f	E_j^f
1	$C_2H_2 + O \leftrightarrows HCCO + H$	5.0×10^{12}	0.0	3200.0
2	$C_2H_2 + O \leftrightarrows CH_2 + CO$	1.5×10^{11}	0.0	3200.0
3	$C_2H_2 + OH \leftrightarrows CH_2CO + H$	3.2×10^{12}	0.0	200.0
4	$C_2H_2 + H \leftrightarrows C_2H + H_2$	2.0×10^{14}	0.0	19000.0
5	$C_2H_3 + M \leftrightarrows C_2H_2 + H + M$	7.94×10^{14}	0.0	31500.0
6	$C_2H_3 + H \leftrightarrows C_2H_2 + H_2$	8.0×10^{12}	0.0	0.0
7	$C_2H_3 + O \leftrightarrows CH_2CO + H$	1.0×10^{13}	0.0	0.0
8	$C_2H_3 + OH \leftrightarrows C_2H_2 + H_2O$	5.0×10^{12}	0.0	0.0
9	$CH_2CO + OH \leftrightarrows CH_2O + HCO$	2.8×10^{13}	0.0	0.0
10	$CH_2O + OH \leftrightarrows HCO + H_2O$	7.53×10^{12}	0.0	167.0
11	$CH_2O + H \leftrightarrows HCO + H_2$	3.31×10^{14}	0.0	10500.0
12	$CH_2O + M \leftrightarrows HCO + H + M$	3.31×10^{16}	0.0	81000.0
13	$CH_2O + O \leftrightarrows HCO + OH$	1.81×10^{13}	0.0	3082.0
14	$HCO + OH \leftrightarrows CO + H_2O$	5.0×10^{12}	0.0	0.0
15	$HCO + M \leftrightarrows H + CO + M$	1.6×10^{14}	0.0	14700.0
16	$HCO + H \leftrightarrows CO + H_2$	4.0×10^{13}	0.0	0.0
17	$HCO + O \leftrightarrows OH + CO$	1.0×10^{13}	0.0	0.0
18	$HCO + O_2 \leftrightarrows HO_2 + CO$	3.0×10^{12}	0.0	0.0
19	$CH_2 + O_2 \leftrightarrows CO_2 + H_2$	1.0×10^{11}	0.0	0.0
20	$CH_2 + O_2 \leftrightarrows HCO + OH$	2.86×10^{12}	0.0	2000.0
21	$CH_2 + O_2 \leftrightarrows CO + H_2O$	2.0×10^{11}	0.0	0.0
22	$CH_2 + O_2 \leftrightarrows CO + OH + H$	2.0×10^{11}	0.0	0.0
23	$CH_2 + O_2 \leftrightarrows HCO + OH$	1.0×10^{11}	0.0	0.0
24	$CO + O + M \leftrightarrows CO_2 + M$	3.2×10^{13}	0.0	−4200.0
25	$CO + OH \leftrightarrows CO_2 + H$	1.26×10^{7}	1.3	−800.0
26	$CO + O_2 \leftrightarrows CO_2 + O$	1.6×10^{13}	0.0	41000.0
27	$C_2H_2 + OH \leftrightarrows C_2H + H_2O$	6.3×10^{12}	0.0	7000.0
28	$C_2H_2 + O \leftrightarrows C_2H + OH$	3.16×10^{15}	0.6	15000.0
29	$C_2H + O_2 \leftrightarrows HCO + CO$	1.0×10^{13}	0.0	7000.0
30	$CH_2 + O \leftrightarrows CH + OH$	2.0×10^{11}	0.68	25000.0
31	$CH_2 + O \leftrightarrows CO + H + H$	3.9×10^{13}	0.0	0.0
32	$CH_2 + O \leftrightarrows CO + H_2$	3.9×10^{13}	0.0	0.0
33	$CH_2 + H \leftrightarrows CH + H_2$	2.51×10^{11}	0.67	25700.0
34	$CH_2 + OH \leftrightarrows CH + H_2O$	2.5×10^{11}	0.67	25700.0
38	$CH_3 + OH \leftrightarrows CH_2O + H_2$	7.5×10^{12}	0.0	0.0
39	$CH_2CO + M \leftrightarrows CH_2 + CO + M$	1.0×10^{17}	0.0	60000.0
40	$C_2H_2 + O_2 \leftrightarrows CH_2CO + O$	1.0×10^{13}	0.0	19000.0

Table continued

TABLE IX (*continued*)

j	Reaction	A_j^f	β_j^f	E_j^f
41	$C_2H_2 + M \leftrightarrows C_2H + H + M$	4.15×10^{16}	0.0	53850.0
42	$CH_2CO + O \leftrightarrows HCCO + OH$	5.0×10^{12}	0.0	0.0
43	$CH_2CO + OH \leftrightarrows HCCO + H_2O$	3.0×10^{13}	0.0	0.0
44	$CH_2CO + H \leftrightarrows HCCO + H_2$	5.0×10^{12}	0.0	0.0
45	$HCCO + O \leftrightarrows HCO + CO$	5.0×10^{12}	0.0	0.0
46	$HCCO + OH \leftrightarrows CH_2O + CO$	2.0×10^{12}	0.0	10000.0
47	$HCCO + OH \leftrightarrows HCO + H + CO$	5.0×10^{12}	0.0	0.0
48	$HCCO + H \leftrightarrows CH_2 + CO$	5.0×10^{12}	0.0	0.0
49	$HCCO + O_2 \leftrightarrows CO_2 + CO + H$	1.0×10^{13}	0.0	5000.0
50	$O_2 + HCCO \leftrightarrows OH + CO + CO$	2.0×10^{12}	0.0	10000.0
51	$O + HCCO \leftrightarrows H + CO + CO$	1.2×10^{12}	0.0	0.0
52	$OH + C_2H_2 \leftrightarrows CH_3 + CO$	5.5×10^{13}	0.0	13700.0
53	$HO_2 + CO \leftrightarrows CO_2 + OH$	1.0×10^{14}	0.0	23000.0
54	$H_2 + O_2 \leftrightarrows 2OH$	1.7×10^{13}	0.0	47780.0
55	$H_2 + OH \leftrightarrows H_2O + H$	5.2×10^{13}	0.0	6500.0
56	$H + O_2 \leftrightarrows OH + O$	7.16×10^{16}	−0.861	16523.0
57	$O + H_2 \leftrightarrows OH + H$	1.8×10^{10}	1.0	8826.0
58	$H + O_2 + M \leftrightarrows HO_2 + M$ H_2O enhanced by 19.0	2.1×10^{18}	−1.0	0.0
59	$OH + HO_2 \leftrightarrows H_2O + O_2$	5.0×10^{13}	0.0	1000.0
60	$H + HO_2 \leftrightarrows 2OH$	2.5×10^{14}	0.0	1900.0
61	$O + HO_2 \leftrightarrows O_2 + OH$	4.8×10^{13}	0.0	1000.0
62	$2OH \leftrightarrows O + H_2O$	6.0×10^{8}	1.3	0.0
63	$H_2 + M \leftrightarrows H + H + M$ H_2O enhanced by 6.0 H enhanced by 2.0 H_2 enhanced by 3.0	2.23×10^{12}	0.5	92600.0
64	$O_2 + M \leftrightarrows O + O + M$	1.85×10^{11}	0.5	95560.0
65	$H + OH + M \leftrightarrows H_2O + M$	7.5×10^{23}	−2.6	0.0
66	$H + HO_2 \leftrightarrows H_2 + O_2$	2.5×10^{13}	0.0	700.0
67	$HO_2 + HO_2 \leftrightarrows H_2O_2 + O_2$	2.0×10^{12}	0.0	0.0
68	$H_2O_2 + M \leftrightarrows OH + OH + M$	1.3×10^{17}	0.0	45500.0
69	$H_2O_2 + H \leftrightarrows HO_2 + H_2$	1.6×10^{12}	0.0	3800.0
70	$H_2O_2 + OH \leftrightarrows H_2O + HO_2$	1.0×10^{13}	0.0	1800.0

Note. $k_j^f = A_j^f T^{\beta_j^f} e^{-E_j^f/RT}$ (units are moles, cm^3, sec).

ACKNOWLEDGMENTS

The author would like to thank Drs. R. J. Kee and J. A. Miller for suggesting the problem and for their continuing support and valuable suggestions concerning this material. The author would also like to thank Drs. S. B. Margolis and T. A. Manteuffel for their helpful comments and suggestions.

REFERENCES

1. J. A. MILLER, R. E. MITCHELL, M. D. SMOOKE, AND R. J. KEE, "Toward a Compehensive Chemical Kinetic Mechanism for the Oxidation of Acetylene: Comparison of Model Predictions with Results from Flame and Shock Tube Experiments," submitted to the 19th Symposium (International) on Combustion, 1982.
2. J. O. HIRSCHFELDER, C. F. CURTISS, AND D. F. CAMPBELL, *J. Phys. Chem.* **57** (1953), 403.
3. D. B. SPALDING, *Philos. Trans. R. Soc. London* **249A** (1956), 1.
4. G. K. ADAMS AND G. B. COOK, *Combust. Flame* **4** (1959), 9.
5. G. DIXON-LEWIS, *Proc. R. Soc. London* **298A** (1967), 495.
6. C. K. WESTBROOK AND F. L. DRYER, *Combust. Sci. Technol.* **20** (1979), 125.
7. C. K. WESTBROOK AND F. L. DRYER, *Combust. Flame* **37** (1980), 171.
8. D. B. SPALDING AND D. L. STEPHENSON, *Proc. R. Soc. London* **324A** (1971), 315.
9. L. BLEDJIAN, *Combust. Flame* **20** (1973), 5.
10. S. B. MARGOLIS, *J. Comput. Phys.* **27** (1978), 410.
11. G. DIXON-LEWIS, *Proc. R. Soc. London* **317A** (1970), 235.
12. K. A. WILDE, *Combust. Flame* **18** (1972), 43.
13. R. M. KENDALL AND J. T. KELLY, Aerotherm TR-75-158 (1975).
14. R. BULIRSCH, J. STOER, AND P. DEUFLHARD, "Numerical Solution of Nonlinear Two-Point Boundary Value Problems I," Numer. Math. Handbook Series Approximation, 1976.
15. I. GLADWELL, "The Development of the Boundary-Value Codes in the Ordinary Differential Equations Chapter of the NAG Library," presented at the Working Conference for Codes for Boundary Value Problems in ODE's, Houston, 1978.
16. M. L. SCOTT AND H. A. WATTS, *SIAM J. Numer. Anal.* **14** (1977), 40.
17. V. PEREYRA, "PASVA3: An Adaptive Finite Difference FORTRAN Program for First Order Nonlinear, Ordinary Boundary Problems," presented at the Working Conference for Codes for Boundary Value Problems in ODE's, Houston, 1978.
18. U. ASCHER, J. CHRISTIANSEN, AND R. D. RUSSELL, "COLSYS—A Collocation Code for Boundary Value Problems," presented at the Working Conference for Codes for Boundary Value Problems in ODE's, Houston (1978).
19. H. B. KELLER, "Numerical Methods for Two-Point Boundary Value Problems," Ginn (Blaisdell), Boston, 1968.
20. S. M. ROBERTS AND J. S. SHIPMAN, "Two-Point Boundary Value Problems: Shooting Methods," Amer. Elsevier, N. Y. (1972).
21. S. B. MARGOLIS, *Quart. Appl. Math.* **38** (1980), 61.
22. K. H. EBERIUS, K. HOYERMANN, AND H. GG. WAGNER, *in* "Proceedings, Thirteenth Symposium (International) on Combustion," The Combustion Institute, 713, Pittsburgh, 1971.
23. J. F. HOLT, *Commun. ACM* **1** (1964), 366.
24. M. LENTINI AND V. PEREYRA, *SIAM. J. Numer. Anal.* **14** (1977), 91.
25. J. O. HIRSCHFELDER AND C. F. CURTISS, *J. Chem. Phys.* **17** (1949), 1076.
26. C. F. CURTISS AND J. O. HIRSCHFELDER, *J. Chem. Phys.* **17** (1949), 550.
27. T. P. COFFEE AND J. M. HEIMERL, "A Comparison of Transport Algorithms for Pre-Mixed, Laminar Steady-State Flames," presented at the Fall Meeting of the Western States Section of the Combustion Institute, October 1980.
28. C. R. WILKE, *J. Chem. Phys.* **18** (1950), 517.
29. R. A. SVEHLA, "Estimated Viscosities and Thermal Conductivities of Gases at High Temperatures," NASA Technical Report R-132, 1962.
30. S. CHAPMAN AND T. G. COWLING, "The Mathematical Theory of Non-Uniform Gases," 3rd ed., Cambridge Univ. Press, Cambridge, 1970.
31. F. R. DE HOOG AND R. WEISS, *SIAM J. Numer. Anal.* **13** (1976), 775.
32. F. R. DE HOOG AND R. WEISS, *Comput.* **24** (1980), 227.
33. M. LENTINI, "Boundary Value Problems over Semi-Infinite Intervals," Ph. D. thesis, California Institute of Technology, 1978.

34. M. D. SMOOKE, "An Error Estimate for the Modified Newton Method with Applications to the Solution of Nonlinear Two-Point Boundary Value Problems," *J. Opt. Theory and Appl.*, in press.
35. A. BRANDT, *Math. Comput.* **31** (1977), 333.
36. R. V. SOUTHWELL, "Relaxation Methods in Theoretical Physics," Clarendon, Oxford, 1946.
37. H. B. KELLER, *SIAM J. Numer. Anal.* **11** (1974), 305.
38. J. KAUTSKY AND N. K. NICHOLS, "Equidistributing Meshes with Constraints," Stanford University Report STAN-CS-79-766, September 1979.
39. A. B. WHITE, JR., *SIAM J. Numer. Anal.* **16** (1979), 472.
40. V. PEREYRA AND E. G. SEWELL, *Numer. Math.* **23** (1975), 261.
41. C. E. PEARSON, *J. Math. Phys.* **47** (1968), 134.
42. R. D. RUSSELL AND J. CHRISTIANSEN, *SIAM J. Numer. Anal.* **15** (1978), 59.
43. C. M. ABLOW AND S. SCHECTER, *J. Comput. Phys.* **27** (1978), 351.
44. E. K. DE RIVAS, *J. Comput. Phys.* **10** (1972), 202.
45. V. E. DENNY AND R. B. LANDIS, *J. Comput. Phys.* **9** (1972), 120.
46. A. R. CURTIS, M. J. D. POWELL, AND J. K. REID, *J. Inst. Math. Its Appl.* **13** (1974), 117.
47. A. C. HINDMARSH, "Solution of Block-Tridiagonal System of Linear Equations," Lawrence Livermore Laboratory Report, UCID-30150, 1977.
48. P. DEUFLHARD, *Numer. Math.* **22** (1974), 289.
49. L. MONCHICK AND E. A. MASON, *J. Chem. Phys.* **35** (1961), 1676.
50. JANNAF Thermochemical Tables, Dow Chemical Company, distributed by Clearinghouse for Federal Scientific and Technical Information, PB168370 (1965), and subsequent addenda.
51. S. GORDON AND B. J. MCBRIDE, "Computer Program for Calculation of Complex Chemical Equilibrium Compositions, Rocket Performance, Incident and Reflected Shocks, and Chapmen–Jouquet Detonations," NASA SP-273, 1971.
52. R. J. KEE, J. A. MILLER, AND T. H. JEFFERSON, "CHEMKIN: A General Purpose, Problem Independent Transportable FORTRAN Chemical Kinetics Code Package," Sandia National Laboratories Report SAND80-8003, 1980.
53. N. PETERS (Ed.), "Proceedings of the GAMM Workshop on Numerical Methods in Laminar Flame Propagation," Vieweg-Verlag, Wiesbaden, West Germany, 1982, to appear.
54. M. KUBICEK, V. HLAVACEK, AND M. HOLODNIOK, "Test Examples for Comparison of Codes for Nonlinear Boundary Value Problems in Ordinary Differential Equations," presented at the Working Conference for Codes for Boundary Value Problems in ODE's, Houston, 1978.
55. J. PEETERS AND G. MAHNEN, *in* "Proceedings, Fourteenth Symposium (International) on Combustion," p. 133, The Combustion Institute, Pittsburgh, 1973.
56. K. H. EBERIUS, K. HOYERMANN, AND H. GG. WAGNER, *in* "Proceedings, Fourteenth Symposium (International) on Combustion," p. 147, The Combustion Institute, 1973.
57. J. WARNATZ, *Ber. Bunsenges. Phys. Chem.* **82** (1978), 834.
58. C. K. WESTBROOK, private communication.
59. C. M. LUND, private communication.
60. J. A. MILLER, private communication.
61. G. TSATSARONIS, *Combust. Flame* **33** (1978), 217.
62. R. D. RUSSELL, "Mesh Selection Methods," presented at the Working Conference for Codes for Boundary Value Problem in ODE's, Houston, 1978.